Soft Matter

PAPER

View Article Online
View Journal

Cite this: DOI: 10.1039/d0sm00828a

Rapid-prototyping a Brownian particle in an active bath†

Jin Tae Park,[ab] Govind Paneru,[a] Chulan Kwon,*[c] Steve Granick *[ad] and Hyuk Kyu Pak *[ab]

Particles kicked by external forces to produce mobility distinct from thermal diffusion are an iconic feature of the active matter problem. Here, we map this onto a minimal model for experiment and theory covering the wide time and length scales of usual active matter systems. A particle diffusing in a harmonic potential generated by an optical trap is kicked by programmed forces with time correlation at random intervals following the Poisson process. The model's generic simplicity allows us to find conditions for which displacements are Gaussian (or not), how diffusion is perturbed (or not) by kicks, and quantifying heat dissipation to maintain the non-equilibrium steady state in an active bath. The model reproduces experimental results of tracer mobility in an active bath of swimming algal cells. It can be used as a stochastic dynamic simulator for Brownian objects in various active baths without mechanistic understanding, owing to the generic framework of the protocol.

Received 8th May 2020,
Accepted 13th July 2020

DOI: 10.1039/d0sm00828a

rsc.li/soft-matter-journal

I. Introduction

Active particles, circulating in liquid or gas more rapidly than from ordinary Brownian motion, frequently collide with passive Brownian particles and in this way boost their mobility. Understanding this is central to the problem of swimming bacteria,[1–8] active colloidal particles,[9–11] and even catalytic enzymes.[12–14] Without wishing to minimize the important differences between these systems, they share the common feature that they involve long-range (usually hydrodynamic) interactions that are difficult or impossible either to control experimentally or compute theoretically. Complexity of the usual systems[4,15,16] precludes one from varying the relevant variables independently; for example, in the bacteria bath, it is not feasible to independently vary the activity of the bacteria, their concentration, and collision times with passive particles. As a result, while experimentally the probability distribution functions of particle position and displacement in bacteria systems are Gaussian in some studies and non-Gaussian in others, the relevant differences of experimental conditions are unclear[17] and analysis is problematical. Here we present a minimal model in which, experimentally and analytically, the relevant variables of the active bath are varied independently without the need for mechanistic understanding of the system. We address the strongly-overdamped situation in which momentum is a second-order effect life at low Reynolds numbers.[18]

To model how active force modulates a thermal system,[19,20] we consider a sphere in the harmonic potential of an optical trap[21] and immersed in viscous liquid. We impose an active force produced by kicks, each of which is exerted randomly in time and decays afterwards. In experiment, the active force is generated by shifting the position of the trap center for a programmed duration time (Fig. 1a). Until another kick comes, the system reverts towards equilibrium by diffusing through the viscous bath. The simplicity of this rapid-prototyping protocol allows us to study directly the interplay between active and thermal forces, varying them independently as cannot be done in most physical systems.

We consider 1D dynamics of a tracer particle in a harmonic trap in the presence of thermal fluctuating force $\xi_{th}(t)$ and active fluctuating force $\xi_{act}(t)$ due to random kicks. In this case, the corresponding equation of motion is given by

$$\gamma\dot{x} = -kx(t) + \xi_{th}(t) + \xi_{act}(t). \quad (1)$$

Here, k is the stiffness of the harmonic potential, and γ is the dissipation coefficient representing solvent viscosity. The thermal force is white noise with zero mean and no memory. Without the active force, the system trivially has a single time constant $\tau_k = \gamma/k$, which is the equilibration time of the particle position in the harmonic potential. We impose an active force generated by a compound Poisson process and parameterized by τ_p (average time interval between kicks), τ_c (kick duration) and X (root-mean-square of random kick amplitude). Considering the process with random

[a] Center for Soft and Living Matter, Institute for Basic Science (IBS), Ulsan 44919, South Korea. E-mail: sgranick@gmail.com, hyuk.k.pak@gmail.com
[b] Department of Physics, Ulsan National Institute of Science and Technology (UNIST), Ulsan 44919, South Korea
[c] Department Physics, Myongji University, Yongin, Gyeonggi-Do 17058, South Korea. E-mail: ckwon58@gmail.com
[d] Department of Chemistry, Ulsan National Institute of Science and Technology (UNIST), Ulsan 44919, South Korea

† Electronic supplementary information (ESI) available. See DOI: 10.1039/d0sm00828a

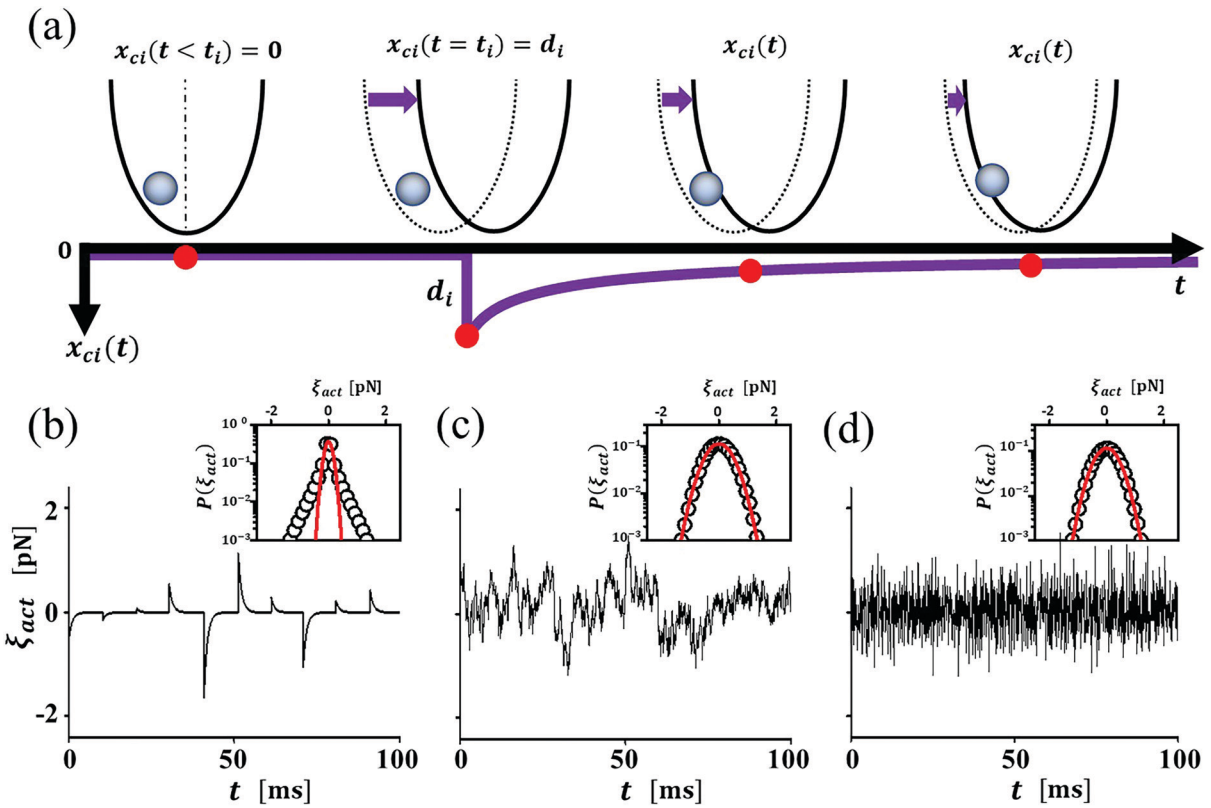

Fig. 1 Generation of active forces. (a) Time-dependent trap center position $x_{ci}(t)$ for ith kick event. Temporal properties of the active force are controlled by the parameters τ_p and τ_c. Here, at $t = t_i$, the trap center position is shifted from 0 to random kick position d_i with variance X^2 and the particle subsequently relaxes towards equilibrium by diffusion through the viscous liquid. Here, $x_{ci}(t < t_i) = 0$ is chosen for the convenience of explaining the effect only from a single kick and its relaxation. But in real experiment usually $x_{ci}(t < t_i) \neq 0$ due to the previous history of kicks with relaxations. Three extreme cases are (b) Poisson correlated active forces when $0 < \tau_c < \tau_p$, (c) Gaussian correlated active forces when $\tau_c \gg \tau_p$, and (d) white noise in the limit of $\tau_c \to 0$ and $\tau_c \to \sqrt{\tau_p}$. Insets are schematic sketches of the probability distribution functions of active force ξ_{act} and Gaussian fits to those curves (red solid curves).

(Poisson) arrival time, τ_p is the average Poisson time.[22,23] In the following, we generate kicks to have random amplitude with equal probability in both directions, such that the kick strength follows a Gaussian distribution with zero mean and variance X^2. Each kick arriving at the time t_i instantaneously shifts the trap center by x_{ci} which has a random amplitude d_i with variance X^2 and decays exponentially with time constant τ_c, as illustrated in Fig. 1a. Then, the position of the trap center at given time $x_c(t)$ is the sum of the past shifted positions of the center of the harmonic trap potential surviving until the next collision, given as

$$x_c(t) = \sum_i d_i e^{-(t-t_i)/\tau_c} \theta(t - t_i). \quad (2)$$

The simplicity of this rapid-prototyping protocol allows us to immediately reproduce many known features of the active matter problem. Time correlation of the active fluctuation force $\xi_{act}(t) = kx_c(t)$ decays exponentially in steady-state for time much larger than τ_c as in other active matter systems,[1,13] $\langle \xi_{act}(t)\xi_{act}(s)\rangle = (k^2X^2\tau_c/2\tau_p)e^{-|t-s|/\tau_c}$ which is derived in ESI.† From eqn (2), we can show that the active force here follows the compound Poisson process

$$\dot{\xi}_{act}(t) = -\xi_{act}(t)/\tau_c + k\sum_{i=1}^{n} d_i\delta(t - t_i). \quad (3)$$

This relation is superficially similar to Ornstein-Uhlenbeck (OU) noise, in which external noise ξ_{ou} is governed by a hidden white noise η_w and follows the stochastic equation $\dot{\xi}_{ou} = -\xi_{ou}/\tau_c + \eta_w(t)$ which yields $\langle \xi_{ou}(t)\xi_{ou}(s)\rangle \propto e^{-|t-s|/\tau_c}$.[24] Though ξ_{act} and ξ_{ou} give rise to the same exponential correlation, the former has higher-order cumulants for all orders, while the latter has none. The important difference is that η_w for the OU noise is a continuous white noise, but the corresponding noise for the active force in this work is a discrete pulsed noise $k\sum_{i=1}^{n} d_i\delta(t - t_i)$. It is appealing that this simple model covers not only Poisson but also Gaussian correlated noises approaching to white noise in a particular limit, as shown in Fig. 1b–d. For the case of short force duration with $\tau_c < \tau_p$, the probability distribution function (PDF) of the active force is non-Gaussian except for short displacements around the center where it follows a Gaussian distribution (inset of Fig. 1b). In the limit $\tau_c/\tau_p \to \infty$, the kick duration greatly exceeds the interval between kicks and the active force becomes a continuous correlated Gaussian noise due to the random nature of d_i with zero mean and the OU noise is recovered (Fig. 1c).[25] We can show that the kurtosis $\propto \tau_p/\tau_c$ vanishes in this limit, which is a signal of the OU noise. A rigorous proof for the transition to the OU noise is given in eqn (S6)–(S9) in ESI.† White noise is also recovered strictly for

very short force duration times (the limit $\tau_c \to 0$) and the condition of $\tau_p \to \tau_c^2$ (Fig. 1d).[26]

II. Materials and methods

Fig. 2 shows the basic scheme of the experimental setup (more details in ESI†).[27,28] The harmonic potential which the tracer particle feels is created by using a computer-controlled optical tweezers, in which a 1064 nm laser is used for trapping the particle. To generate the time-dependent active force, the laser beam is fed through an acoustic optical deflector (AOD) which is controlled dynamically *via* a computer. The AOD is properly mounted at the back focal plane of the objective lens (100×, Oil, NA: 1.4) so that the stiffness of the potential k is essentially constant while shifting the position of the trap center at the speed of 5 kHz. A second laser with 980 nm wavelength is used for tracking the particle position. A quadrant photodiode (QPD) is used to measure the particle position by detecting the scattered tracking laser light from the particle with the accuracy of 1 nm and at the rate of 5 kHz. The sample cell consists of a highly diluted solution of 2.0 μm diameter polystyrene spheres suspended in deionized water. The volume fraction of the particles is $\phi = 2.0 \times 10^{-6}$. All experiments were carried out at 295 ± 0.1 K. In this experiment, the trap stiffness is k = 15.4 pN μm and the characteristic relaxation time is $\tau_k = \gamma/k \cong 1.1$ ms.

III. Results and discussion

A. Enhanced Gaussian or non-Gaussian diffusion in an active bath

The mean square displacement (MSD) during time interval t in steady-state can be found by using the time-correlation of the active force, given as

$$\langle \Delta x^2(t) \rangle = 2(k_B T/k)\left(1 - e^{-t/\tau_k}\right) + 2(k_B T_{act}/k)\frac{\left[1 - e^{-t/\tau_k} - (\tau_c/\tau_k)\left(1 - e^{-t/\tau_c}\right)\right]}{(1 - \tau_c/\tau_k)}. \quad (4)$$

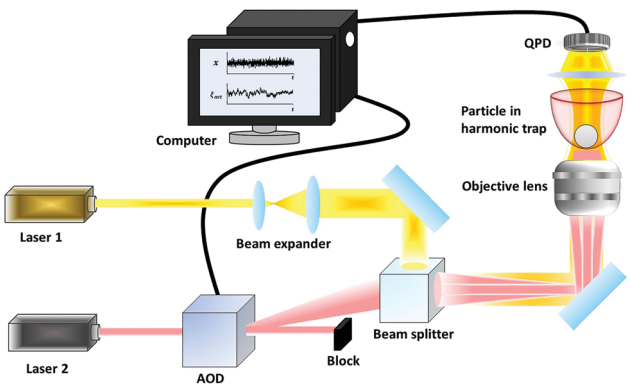

Fig. 2 Schematic diagram of experimental set up. The Laser1 (λ = 980 nm) and Laser2 (λ = 1064 nm) are tracking and trapping lasers, respectively. A colloidal sphere is trapped inside the optical harmonic potential generated by the trapping beam which is manipulated by the combination of AOD (acoustic optical deflector) and computer. The QPD (quadrant photodiode) detects the position of particle and its signal is sent to computer.

Here, $T_{act} = kX^2\tau_c^2/[2k_B\tau_p\tau_k(1 + \tau_c/\tau_k)]$ is "tracer activity" which quantifies how active forces modulate mobility, in a similar spirit to the phrase "active temperature" used elsewhere.[29] Trivially, MSD is governed only by the thermal diffusion coefficient $D_{th} = k_BT/\gamma$ for time much less than τ_c and τ_k, given as $2D_{th}t$. In a long time limit, the MSD is $\langle \Delta x^2(t) \rangle = 2(k_B/k)(T + T_{act})$ where $D_{act} = k_BT_{act}/\gamma$ plays the formal role of active diffusion coefficient.[30] The model is formulated such that thermal and active forces split into independent contributions.[29]

Fig. 3a shows the MSD curves for various conditions. The black open circles are the MSD measurements at thermal equilibrium for $X^2 = 0$. All other colored open circles correspond to the experimental MSD data in non-equilibrium steady-state conditions with different values of τ_p, but other parameter values fixed. All data agree with the theoretical predictions given in eqn (4). As the average interval time between kicks is decreased, the number of collision events τ_c/τ_p and the activity T_{act} increase. Therefore, the saturating value of the MSD, $2\langle \Delta x^2(t) \rangle$ in Fig. 3a, increases with T_{act} suggesting enhanced diffusion due to the active force.[31] The violet dotted line indicates the slope of unity for free diffusion.

The open circles in Fig. 3b are the PDFs of the particle position $P(x)$ in steady-state at fixed τ_c and X. For $\tau_c/\tau_p \gtrsim 1$, $P(x)$ follows a Gaussian distribution. For $\tau_c/\tau_p < 1$, $P(x)$ shows a non-Gaussian behavior. In this case, $P(x)$ has a Gaussian shape near the center but an exponential behavior at tails. The degree of non-Gaussianity of $P(x)$ can be quantified by measuring a non-Gaussian parameter,[32] defined as $\alpha_2 \equiv [\langle x^4 \rangle/5\langle x^2 \rangle^2] - 3/5$, as shown in the inset of Fig. 3b. According to this, for $\tau_c/\tau_p \gtrsim 1$, $P(x)$ is always Gaussian-like ($\alpha_2 \approx 0$). And, for $0 < \tau_c/\tau_p < 1$, $P(x)$ is non-Gaussian ($\alpha_2 > 0$). But, in the limit $\tau_c/\tau_p \approx 0$, $P(x)$ becomes Gaussian ($\alpha_2 \approx 0$) again. These results agree with previous experiments in which the PDF becomes non-Gaussian when the concentration of active particles is low, corresponding to $\tau_c/\tau_p < 1$ in our experiment.[7]

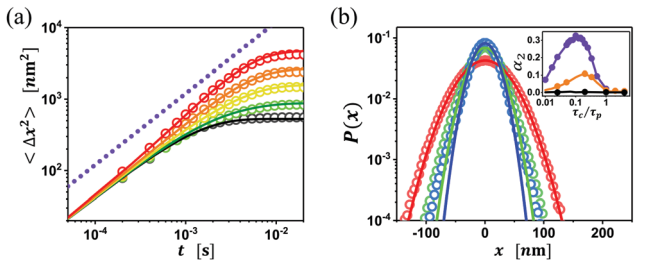

Fig. 3 Mean square displacement (MSD) and probability distribution function (PDF) of particle in active bath. (a) MSDs are plotted against time on log-log scales, for various τ_c/τ_p: 4.0 (red), 2.0 (orange), 1.0 (yellow), and 0.33 (green). The black curve corresponds to MSD without active force. Here, X = 37 nm, τ_c = 4 ms and τ_k = 1.1 ms. The circles are experimental results and the solid curves are predictions using eqn (4). The dotted line shows the slope of unity corresponding to free diffusion. (b) PDFs are plotted for τ_c/τ_p: 1.0 (red), 0.33 (green), and 0.2 (blue) for X = 70 nm and τ_c = 2 ms. The solid curves are Gaussian fits. The inset plots the non-Gaussian parameter α_2 against τ_c/τ_p. The solid circles are from experiments and the solid curves are from eqn (4). Here, X = 70 nm (violet), 37 nm (orange), 20 nm (black) and τ_c = 2 ms (violet, black), 4 ms (orange).

These observations can be explained by using the property of no-correlation between thermal and active forces that the particle position can be separated into non-thermal part x_{act} exclusively due to the active force and thermal part $x - x_{act}$. Therefore, $P(x)$ can be expressed as the convolution of $P(x_{act})$ and $P(x - x_{act})$, $P(x) = \int P(x - x_{act})P(x_{act})dx_{act}$ (see Fig. S1 in ESI†).[33] Here, $P(x - x_{act}) = \sqrt{k/2\pi k_B T}e^{-k(x-x_{act})^2/2k_B T}$. The essential ingredient for non-Gaussian $P(x)$ is that $P(x_{act})$ is non-Gaussian ($\tau_c/\tau_p < 1$). However, if the tails of $P(x_{act})$ do not surpass roughly 4σ (4 standard deviations) of $P(x - x_{act})$, $P(x)$ still shows a Gaussian behavior to the eye (see Fig. S1 in ESI†), because the equilibration process of the particle position inside the harmonic potential wipes out the non-Gaussian effect of the active force. Even though $P(x)$ is Gaussian in this regime, the van Hove self-correlation function, $G_s(\Delta x,\Delta t)$, which is the PDF of the particle displacement Δx during Δt, shows non-Gaussian behavior at shorter times (see Fig. S2 in ESI†). A recent theory explains the non-Gaussian tail by considering the hydrodynamic interactions between the tracer particle and the active particles, with the active force that arrives at random (Poisson) intervals.[34] The approach taken here complements that rigorous but complex analysis by using a rapid prototyping formalism.

B. Comparison with real bio-active bath experiment

There were many experimental studies of real bio-active bath.[35–39] Among them, the experimental study of the tracer-particle diffusion in a quasi-two-dimensional bath of swimming algal cells (Chlamydomonas) by J. Gollub *et al.*,[3] is compared with the simulation study using our model. This work is chosen because they measured MSD and van Hove correlation function of tracer particles which we are interested in for various cell concentrations.[3] The cell volume fraction Φ was controlled from Φ = 0.3% to 7% and $G_s(\Delta x,\Delta t)$ accordingly changes from highly non-Gaussian to Gaussian (colored circles in Fig. 4a). Since there is no harmonic trap ($k = 0$) in the experiment, eqn (1) becomes $\gamma\dot{x} = \xi_{th}(t) + \xi_{act}(t)$. The corresponding MSD can be found as (see derivation in ESI†)

$$\langle \Delta x^2(t)\rangle = 2D_{th}t + 2D_{act}[t - \tau_c(1 - e^{-t/\tau_c})], \qquad (5)$$

where diffusion coefficients are given as $D_{th} = k_B T/\gamma$ for thermal noise and $D_{act} = f_{RMS}{}^2\tau_c{}^2/(2\gamma^2\tau_p)$ for active force. Here, the root-mean-square (RMS) kicking force kX is replaced by f_{RMS} and $\langle \xi_{act}(t)\xi_{act}(0)\rangle = f_{RMS}{}^2\tau_c/(2\tau_p)e^{-t/\tau_c}$ (see derivation in ESI†). By fitting eqn (5) to the MSD data of the experiment, we can estimate the values of τ_c = 300 ms and D_{act} for various values of Φ. In the computer simulation using our model, $G_s(\Delta x,\Delta t)$ (solid curves) agrees well with the experimental data (colored circles) when f_{RMS} = 0.4 pN and $\tau_p \sim \Phi^{-3/2}$ are used (Fig. 4a). Here, $G_s(\Delta x,\Delta t)$ becomes Gaussian (non-Gaussian) when the cell concentration is high (low), corresponding to $\tau_c/\tau_p \gtrsim 1$ ($\tau_c/\tau_p < 1$). This observation agrees with the argument in the last section. When active diffusion dominates over thermal diffusion, the effective diffusion coefficient, $D_{eff} = D_{th} + D_{act}$ is approximately equal to $D_{eff} \approx D_{act} \sim \tau_p{}^{-1}$. Fig. 4b shows an excellent agreement of $D_{eff} \sim \tau_p{}^{-1}$ from our simulation with

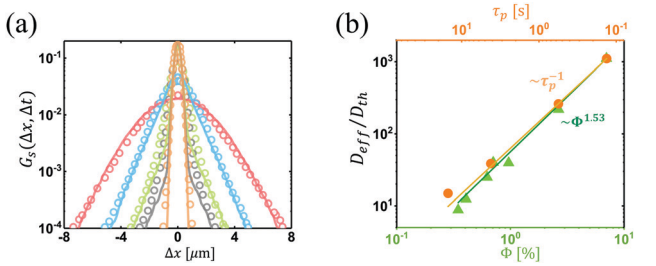

Fig. 4 Comparison between active force model and the experimental data of algal cell active bath. (a) The van Hove self-correlation function during a fixed short time interval (Δt = 0.04 s) at various volume fractions: Φ = 7.0% (red), 2.7% (blue), 0.7% (green), 0.3% (gray) and Φ = 0% (orange). The circles are from the experiment and the solid curves are from the simulation results with τ_p = 0.13 s (red), τ_p = 0.56 s (blue), τ_p = 4.2 s (green) and τ_p = 15 s (gray) at fixed τ_c = 0.3 s and f_{RMS} =0.4 pN. (b) The effective diffusion coefficient D_{eff} normalized by thermal diffusion coefficient D_{th} for various volume fractions Φ in experiment and corresponding kick intervals $\tau_p$in simulation. Here, the triangles (experiment) are fitted with $D_{eff} \sim \Phi^{1.53}$ and the circles (simulation) with $D_{eff} \sim \tau_p{}^{-1}$.

$D_{eff} \sim \Phi^{3/2}$ from the experiment. The relation $\tau_p \sim \Phi^{-3/2}$ can be explained by the assumption that the average kick interval is inversely proportional to the concentration of the active particles ($\Phi^{3/2}$) in a two-dimensional active bath. The observed mean speed of the cells was $v_0 \approx 100$ μm s^{-1} in experiment, therefore f_{RMS} is roughly the magnitude of the drag force which the tracer particle feels when the speed of a tracer particle is of the same order of magnitude as that of a cell as they drag each other, $f_{RMS} \approx \gamma v_0 \approx$ 0.4 pN. This comparison suggests that even though our simple model does not include the details about the active bath, such as hydrodynamic interactions between the tracer particle and active particles[34] and among the active particles, it can explain the enhanced diffusion and non-Gaussian statistics in real bio-active bath very well.

C. Heat dissipation in an active bath

We now investigate the heat dissipation in an active bath using the model described above. Due to the energy balance between continual energy input (work) and simultaneous energy dissipation to (at) the thermal bath,[40] the first law of thermodynamics is $dE/dt = \dot{W} - \dot{Q}$. Based on the view of the potential with perturbed center by active noise, the internal energy E is equal to $k(x - \xi_{act}(t)/k)^2/2$. In this situation, the rate of work done by the external agent producing active noises is known to be equal to $\dot{W} = \partial E/\partial t = -(x - \xi_{act}/k)\dot{\xi}_{act}$. Different definitions of internal energy and work can be used, but the rate of heat dissipation is uniquely defined as $\dot{Q} = (\gamma\dot{x} - \xi_{th})\dot{x}$. In non-equilibrium steady state, $\langle dE/dt\rangle = 0$, so $\langle\dot{W}\rangle = \langle\dot{Q}\rangle$, independent of the definition of heat. Theoretically, one can find $\langle\dot{Q}\rangle = k_B T_{act}/\tau_c$, which is derived in ESI.† To quantify this experimentally, we used the recent seminal work by Harada and Sasa,[41] in which the average rate of heat dissipation $\langle\dot{Q}\rangle$ is related to experimentally accessible quantities *via* a fluctuation-dissipation relation.[42–44]

$$\langle\dot{Q}\rangle = \frac{\gamma}{2\pi}\int_{-\infty}^{\infty} d\omega[C(\omega) - 2k_B TR(\omega)] \qquad (6)$$

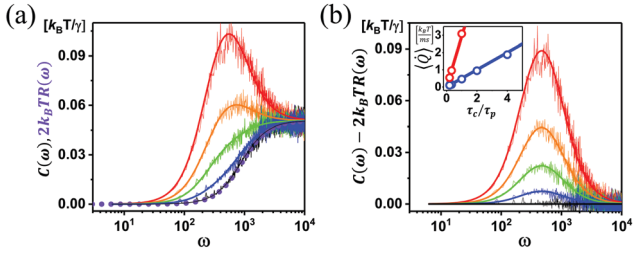

Fig. 5 Measurement of heat dissipation rate, $\langle \dot{Q} \rangle$. (a) Correlation function $C(\omega)$ and response function $2k_BTR(\omega)$ of systems under various conditions. Here, τ_c/τ_p: 4.0 (red), 2.0 (orange), 1.0 (green), and 0.33 (blue) with fixed values of τ_c = 4 ms and X = 37 nm. The smooth and thick solid curves are theoretical predictions for $C(\omega)$ and the noisy curves are corresponding experimental ones. The violet dashed and solid curves are the experimental and theoretical response functions. It is the same regardless of the active force. (b) Semi-log plot of spectral heat dissipation rate $C(\omega) - 2k_BTR(\omega)$ *vs.* frequency ω for the data in (a), in which τ_c value is fixed. Inset plots the total heat dissipation rate $\langle \dot{Q} \rangle$ against τ_c/τ_p. The open circles are experimental measurements and the solid curves are the theoretical prediction, k_BT_{act}/τ_c. Here, red (blue) color corresponds to X = 70 nm (37 nm) and τ_c = 2 ms (4 ms).

Here, $C(\omega)$ is the velocity auto-correlation function and $R(\omega)$ is the real part of the response function for the velocity measurement in frequency space.

The integrand in eqn (6) can be measured directly in our experiment. The noisy thin solid lines in Fig. 5a are the measurements of $C(\omega)$ and $2k_BTR(\omega)$[45] for various conditions; the experimental detail can be found in ESI.† The solid thick curves are the theoretical predictions. In the equilibrium condition where T_{act} = 0, $C(\omega)$ and $2k_BTR(\omega)$ are superimposed satisfying the typical fluctuation-dissipation relation. As T_{act} increases, however, $C(\omega)$ differs increasingly from $2k_BTR(\omega)$. $C(\omega)$ is the effect of the velocity fluctuation of the particle to increase with T_{act}, while the response function $R(\omega)$ is the property independent of zero mean active force, hence independent of T_{act}.[46]

Fig. 5b shows $C(\omega) - 2k_BTR(\omega)$ which is proportional to the spectral heat dissipation rate at given frequency ω from the data in Fig. 5a, where the correlation time τ_c is fixed but τ_c/τ_p is varied. The area under each curve is proportional to the average value of the total heat dissipation rate $\langle \dot{Q} \rangle$ at that condition. The inset of Fig. 5b shows that the measured $\langle \dot{Q} \rangle$ agrees well with the theoretical prediction k_BT_{act}/τ_c. All results related to the heat dissipation rate measurements are valid for not only Gaussian but also non-Gaussian $P(x)$. Maximum rate of heat dissipation occurs at the frequency $\omega_d = (\tau_c\tau_k)^{-1/2}$. This seems natural because τ_k is the characteristic equilibration time for the particle position to be randomized inside the harmonic potential and τ_c is the characteristic duration time of the active force which represents the duration of energy input by the active force.

IV. Conclusions

In summary, we demonstrated a new experimental and theoretical approach using a rapid-prototyping protocol to study systematically Brownian particles in an active bath. Our experiments using an optical trap and numerical and theoretical calculations based on the equation of motion in eqn (1) agree in showing enhanced diffusion that gives rise to non-Boltzmann, hence non-Gaussian PDFs except for the range where the kick duration time is much larger than the average interval time between kicks. Computer simulation using our model agrees with the previously published experimental data of the tracer particle diffusion in the quasi-two-dimensional bath of swimming algal cells. We also measured heat dissipation using the fluctuation–dissipation relation and found that maximum heat dissipation rate occurs at the time-scale of the geometric mean of the kick duration time and the particle thermal equilibration time.

Our study can be used as a stochastic dynamic simulator for both the experiments and computer simulations of Brownian objects in various active baths without the need for mechanistic understanding, owing to the generic framework of this rapid prototyping protocol. This work has not considered those systems that exhibit non-Gaussian behavior at equilibrium. A vast literature considers models to describe such behavior – "strange kinetics",[47] "diffusing diffusivity",[48] continuous-time random walks,[49] phenomenology,[5,50] and much more. In common, those situations share complexity not addressed here. First, the physical environment in those problems is not the simple harmonic potential we posit here. Second, inherent noise at equilibrium is not necessarily white noise. While these features could, in principle, be addressed using the rapid-prototype model introduced here, to do so goes beyond the scope of the present study.

Conflicts of interest

There are no conflicts to declare.

Acknowledgements

This work was supported by the taxpayers of South Korea through the Institute for Basic Science with grant No. IBS-R020-D1 (HKP and SG) and Basic Science Research Program of the National Research Foundation(NRF) funded by the Ministry of Education with grant no. 2020R1A2C100976111 (CK). We thank Profs. Bongsoo Kim and Jae Hyung Jeon for insightful discussion and comments.

References

1 X. L. Wu and A. Libchaber, *Phys. Rev. Lett.*, 2000, **84**, 3017–3020.
2 R. E. Goldstein, M. Polin and I. Tuval, *Phys. Rev. Lett.*, 2009, **103**, 168103.
3 H. Kurtuldu, J. S. Guasto, K. A. Johnson and J. P. Gollub, *Proc. Natl. Acad. Sci. U. S. A.*, 2011, **108**, 10391–10395.
4 C. Bechinger, R. Di Leonardo, H. Löwen, C. Reichhardt, G. Volpe and G. Volpe, *Rev. Mod. Phys.*, 2016, **88**, 045006.
5 B. Wang, S. M. Anthony, S. C. Bae and S. Granick, *Proc. Natl. Acad. Sci. U. S. A.*, 2009, **106**, 15160–15164.
6 L. Dabelow, S. Bo and R. Eichhorn, *Phys. Rev. X*, 2019, **9**, 021009.
7 S. Krishnamurthy, S. Ghosh, D. Chatterji, R. Ganapathy and A. K. Sood, *Nat. Phys.*, 2016, **12**, 1134–1138.

8 G. L. Miño, J. Dunstan, A. Rousselet, E. Clément and R. Soto, *J. Fluid Mech.*, 2013, **729**, 423–444.
9 F. Schmidt, B. Liebchen, H. Lowen and G. Volpe, *J. Chem. Phys.*, 2019, **150**, 094905.
10 F. Kummel, P. Shabestari, C. Lozano, G. Volpe and C. Bechinger, *Soft Matter*, 2015, **11**, 6187–6191.
11 J. Yan, M. Han, J. Zhang, C. Xu, E. Luijten and S. Granick, *Nat. Mater.*, 2016, **15**, 1095–1099.
12 A. Y. Jee, S. Dutta, Y. K. Cho, T. Tlusty and S. Granick, *Proc. Natl. Acad. Sci. U. S. A.*, 2018, **115**, 14–18.
13 A. Y. Jee, Y. K. Cho, S. Granick and T. Tlusty, *Proc. Natl. Acad. Sci. U. S. A.*, 2018, **115**, E10812.
14 J. P. Gunther, G. Majer and P. Fischer, *J. Chem. Phys.*, 2019, **150**, 124201.
15 M. Guo, A. J. Ehrlicher, M. H. Jensen, M. Renz, J. R. Moore, R. D. Goldman, J. Lippincott-Schwartz, F. C. Mackintosh and D. A. Weitz, *Cell*, 2014, **158**, 822–832.
16 F. C. MacKintosh and A. J. Levine, *Phys. Rev. Lett.*, 2008, **100**, 018104.
17 K. C. Leptos, J. S. Guasto, J. P. Gollub, A. I. Pesci and R. E. Goldstein, *Phys. Rev. Lett.*, 2009, **103**, 198103.
18 E. M. Purcell, *Am. J. Phys.*, 1977, **45**, 3–11.
19 I. A. Martínez, É. Roldán, J. M. R. Parrondo and D. Petrov, *Phys. Rev. E: Stat., Nonlinear, Soft Matter Phys.*, 2013, **87**, 032159.
20 A. Bérut, A. Petrosyan and S. Ciliberto, *EPL*, 2014, **107**, 60004.
21 A. Ashkin, J. M. Dziedzic, J. E. Bjorkholm and S. Chu, *Opt. Lett.*, 1986, **11**, 288.
22 K. Kanazawa, *Statistical Mechanics For Athermal Fluctuation: non-Gaussian noise in physics*, Springer, 2018.
23 É. Fodor, H. Hayakawa, J. Tailleur and F. van Wijland, *Phys. Rev. E*, 2018, **98**, 062610.
24 J. R. Gomez-Solano, L. Bellon, A. Petrosyan and S. Ciliberto, *EPL*, 2010, **89**, 60003.
25 N. G. Van Kampen, *Stochastic Processes in Physics and Chemistry*, Elsevier, 3rd edn, 2007, pp. 52–95.
26 K. Kanazawa, T. G. Sano, T. Sagawa and H. Hayakawa, *Phys. Rev. Lett.*, 2015, **114**, 090601.
27 G. Paneru, D. Y. Lee, T. Tlusty and H. K. Pak, *Phys. Rev. Lett.*, 2018, **120**, 020601.
28 G. Paneru, S. Dutta, T. Sagawa, T. Tlusty and H. K. Pak, *Nat. Commun.*, 2020, **11**, 1012.
29 C. Maggi, M. Paoluzzi, N. Pellicciotta, A. Lepore, L. Angelani and R. Di Leonardo, *Phys. Rev. Lett.*, 2014, **113**, 238303.
30 S. Chaki and R. Chakrabarti, *Phys. A*, 2018, **511**, 302–315.
31 É. Fodor, M. Guo, N. S. Gov, P. Visco, D. A. Weitz and F. van Wijland, *EPL*, 2015, **110**, 48005.
32 A. Rahman, *Phys. Rev.*, 1964, **136**, A405–A411.
33 X. He, Y. Wang and P. Tong, *Phys. Rev. Fluids*, 2018, **3**, 052401(R).
34 K. Kanazawa, T. G. Sano, A. Cairoli and A. Baule, *Nature*, 2020, **579**, 364–367.
35 E. Pince, S. K. Velu, A. Callegari, P. Elahi, S. Gigan, G. Volpe and G. Volpe, *Nat. Commun.*, 2016, **7**, 10907.
36 T. Turiv, R. Koizumi, K. Thijssen, M. M. Genkin, H. Yu, C. Peng, Q.-H. Wei, J. M. Yeomans, I. S. Aranson, A. Doostmohammadi and O. D. Lavrentovich, *Nat. Phys.*, 2020, **16**, 481–487.
37 C. Maggi, M. Paoluzzi, L. Angelani and R. Di Leonardo, *Sci. Rep.*, 2017, **7**, 17588.
38 T. Kurihara, M. Aridome, H. Ayade, I. Zaid and D. Mizuno, *Phys. Rev. E*, 2017, **95**, 030601.
39 D. Needleman and Z. Dogic, *Nat. Rev. Mater.*, 2017, **2**, 17048.
40 S. Chaki and R. Chakrabarti, *Phys. A*, 2019, **530**, 121574.
41 T. Harada and S. Sasa, *Phys. Rev. Lett.*, 2005, **95**, 130602.
42 R. Kubo, *Rep. Prog. Phys.*, 1966, **29**, 255–284.
43 L. Bellon, S. Ciliberto and C. Laroche, *Europhys. Lett.*, 2001, **53**, 511–517.
44 R. Zwanzig, *Nonequilibrium statistical mechanics*, Oxford Univ. Press, Oxford, 2009.
45 S. Toyabe, H. R. Jiang, T. Nakamura, Y. Murayama and M. Sano, *Phys. Rev. E: Stat., Nonlinear, Soft Matter Phys.*, 2007, **75**, 011122.
46 E. Dieterich, J. Camunas-Soler, M. Ribezzi-Crivellari, U. Seifert and F. Ritort, *Nat. Phys.*, 2015, **11**, 971–977.
47 M. F. Shlesinger, G. M. Zaslavsky and J. Klafter, *Nature*, 1993, **363**, 31–37.
48 M. V. Chubynsky and G. W. Slater, *Phys. Rev. Lett.*, 2014, **113**, 098302.
49 J. H. P. Schulz, A. V. Chechkin and R. Metzler, *J. Phys. A: Math. Theor.*, 2013, **46**, 475001.
50 B. Wang, J. Kuo, S. C. Bae and S. Granick, *Nat. Mater.*, 2012, **11**, 481–485.

